Journal of Membrane Science 568 (2018) 10–16

Contents lists available at ScienceDirect

Journal of Membrane Science

journal homepage: www.elsevier.com/locate/memsci

# Fabrication of cellulose nanofibrils/UiO-66-$NH_2$ composite membrane for $CO_2/N_2$ separation

Xiong-Fei Zhang[a], Yi Feng[a], Zhongguo Wang[a], Mingmin Jia[a], Jianfeng Yao[a,b,*]

[a] College of Chemical Engineering, Jiangsu Key Lab for the Chemistry & Utilization of Agricultural and Forest Biomass, Nanjing Forestry University, Nanjing 210037, China
[b] Jiangsu Co-Innovation Center of Efficient Processing and Utilization of Forest Resources, Nanjing Forestry University, Nanjing 210037, China

ARTICLE INFO

*Keywords:*
Nanocellulose
UiO-66-$NH_2$
Composite membrane
Gas separation

ABSTRACT

Incorporating metal-organic frameworks into cellulose matrix to prepare composite membranes is promising in gas-separation applications. In this study, UiO-66-$NH_2$ (Zr-based MOF) nanoparticles are wrapped into the densely packed cellulose nanofibrils (CNF-COOH) via a facile vacuum filtration process. The existence of acid-base interactions and electrostatic forces between UiO-66-$NH_2$ and CNF-COOH renders ideal interfacial morphology. Results show that UiO-66-$NH_2$ is cross-linked by -COOH groups and well-dispersed in the CNF matrix. The porous UiO-66-$NH_2$ strengthens the diffusion process of $CO_2$ molecules, thus elevating the permeation flux and separation factor simultaneously. The optimum separation performance is achieved over CM-1 membrane with a $CO_2$ permeability of 139 Barrer and a $CO_2/N_2$ selectivity ratio of 46.

## 1. Introduction

Membrane based gas-separation techniques are one of the key ways to achieve green chemical processes [1]. Metal-organic frameworks (MOFs) have been emerging as a new class of membrane materials distinguished by their high surface area, controllable pore size and versatilities in group modification [1–3]. The difficulty in fabricating pure MOF membranes without defects and voids limits the practical application of MOF materials [4,5]. A promising strategy is to unite inorganic MOFs with polymers, which combines the size/shape sieving effect of MOFs and membrane forming property of the polymer matrix [6,7]. Various polymer/MOF composite membranes containing MOFs such as MOF-5, MIL-101, zeolitic imidazolate frameworks (ZIFs), occupied much attention in the field of gas separation [8,9]. The simple dispersion or mechanical mixing of MOF powders into polymer matrix frequently induces undesirable gas leakage at the interface due to the poor compatibility [10]. UiO-66 (Universitet of Oslo), a zirconium-based MOF, featuring triangular pores of approximately 6 Å, is an attractive candidate for the fabrication of composite membranes as already shown for $CO_2/N_2$ and $CO_2/CH_4$ separation [11,12]. The $CO_2$ binding affinity of UiO-66 can be potentially enhanced through controlled and proper functionalization. However, the problems for poor polymer-MOF affinity, interfacial defects and gas leakage still remain unsolved [8,13,14].

Cellulose nanofibrils (CNFs) are eco-friendly and degradable biomass materials [15,16]. Recently, interests in the fabrication of membranes or nanopapers using CNFs are on continuous rise because of numerous applications ranging from optical devices, electromagnetic shielding, medical carrier, food package and separation [17,18]. 2,2,6,6-tetramethylpiperidine-1-oxyl radical (TEMPO)-oxidized CNFs developed by Isogai's group (the University of Tokyo) exhibited excellent transmittance, high mechanical properties, small width (3–5 nm) and large aspect ratios (200–500) [19,20]. The entangled web-like structures of CNFs is effective to reduce the voids in the membranes. In terms of gas separation, the densely packed membranes consisting of nanosized cellulose fibrils make such membranes excellent matrices for MOFs [10]. The abundant carboxylate groups (-$COO^-$) located on the CNFs provide a possibility for CNFs to cross-link with functional groups on MOFs. We previously reported that UiO-66-$NH_2$ can be intercalated into graphene oxide (GO) nanosheets and the non-selective voids between UiO-66 and GO are effectively avoided [2].

Here, the conjugation of MOFs with flexible CNFs was performed by utilizing CNF-COOH to cross-link UiO-66-$NH_2$. The -$NH_2$ groups of MOF can be easily anchored to -COOH groups through acid-base interaction and electrostatic forces. The host matrix enhances interfacial morphology and the dispersed MOF is cross-linked by the -COOH groups of the cellulose matrix. The porous structure of UiO-66-$NH_2$ offers fast transport channels for $CO_2$ and enhanced $CO_2$ separation performance is expected.

* Corresponding author.
*E-mail address:* jfyao@njfu.edu.cn (J. Yao).

https://doi.org/10.1016/j.memsci.2018.09.055
Received 10 July 2018; Received in revised form 2 September 2018; Accepted 23 September 2018
Available online 25 September 2018

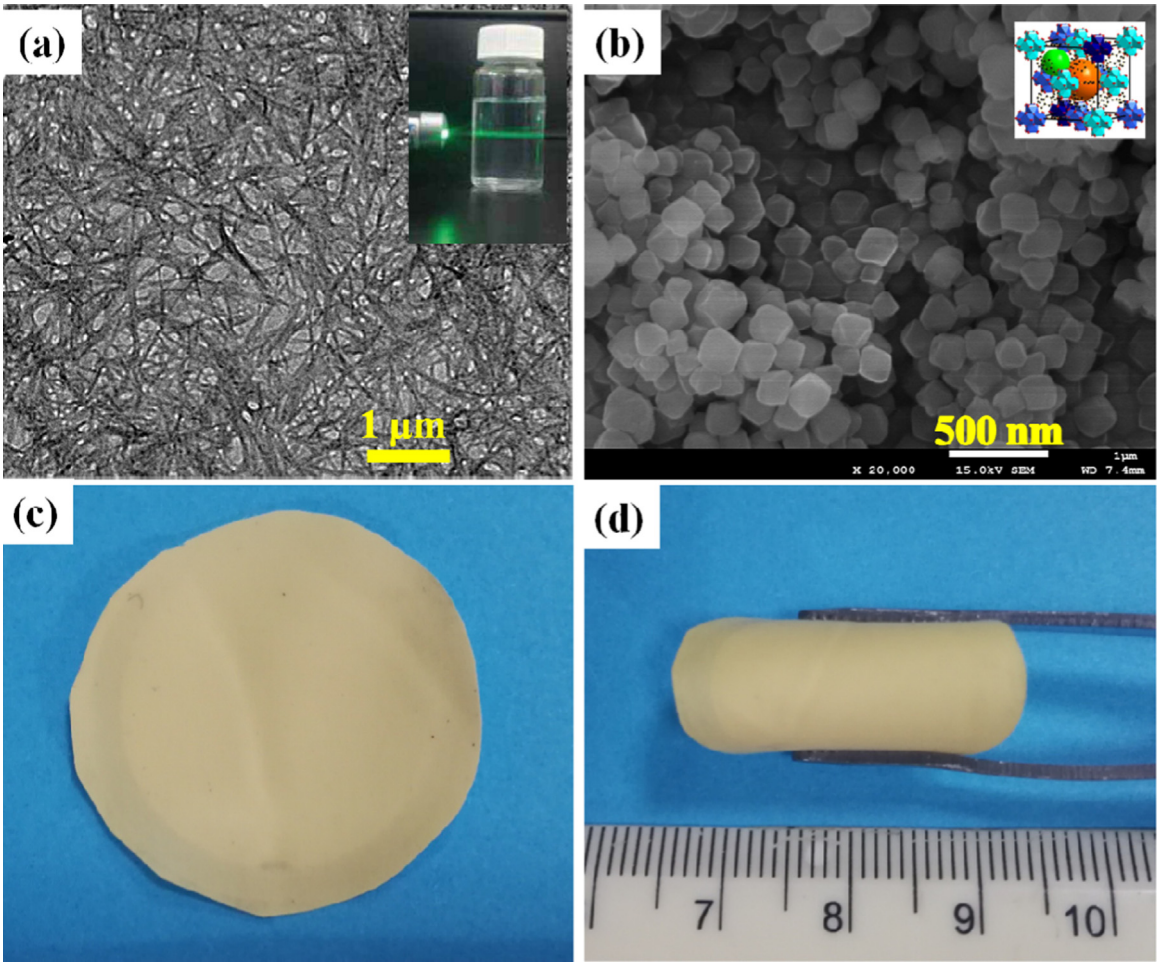


**Fig. 1.** TEM image of the CNFs (a), SEM image of UiO-66-$NH_2$ (b), optical view (c) and bendable behavior (d) of CM-1 membrane.

## 2. Experimental

### 2.1. Materials

TEMPO-oxidized (2,2,6,6-tetramethylpiperidine-1-oxyl radical) cotton cellulose nanofibril suspension (CNF-COONa, 0.6% w/v) was obtained from QiHong Company (Guilin, China). The sodium carboxylate groups (CNF-COONa) can be changed into free protonated carboxyl groups (CNF-COOH) via the facile soaking (0.01 M HCl, pH = 4.5) and successive water washing treatment. Zirconium (IV) chloride ($ZrCl_4$, 98%) was bought from Aladdin Chemical Comapany. 2-Aminoterephthalic acid (ATA, 99.5%), 1,4-benzendicarboxylic acid (BDC, 98%), N,N-dimethyl formamide (DMF, 99.5%), acetic acid (HAc) and ethanol were supplied by Sinopharm Reagent Company. Mixed cellulose ester (MCE, Φ 0.22 μm) filter support was purchased from Xingya Materials Company (Shanghai, China).

### 2.2. Preparation of UiO-66 and UiO-66-$NH_2$

UiO-66 nanocrystals were prepared via solvothermal method as described in our previous work [21]. For the synthesis of UiO-66-$NH_2$, a slight modified method was employed based on literature [2]. In a typical synthesis, 191 mg of $ZrCl_4$ and 146 mg of ATA were added to DMF solution (82 mL). Afterwards, 4.83 g of HAc was added to the mixed solution. The solution with a $ZrCl_4$: ATA: HAc: DMF molar ratio of 1: 1: 100: 500 was stirred for 1 h and subjected to ultrasonic treatment for 10 min for three cycles. The solution was transferred into a Teflon-lined stainless steel autoclave (150 mL) and heated at 120 °C for 24 h. Subsequently, the synthesized UiO-66-$NH_2$ powder was washed by DMF/methanol and dried at 60 °C overnight.

### 2.3. Membrane fabrication

The MOF/CNF composite membranes were fabricated by a vacuum filtration method. Taking UiO-66-$NH_2$/CNF-COOH as an example, predetermined amount (24 mg) of UiO-66-$NH_2$ particle was dispersed in 20 mL water and sonicated for 30 min. The UiO-66-$NH_2$ dispersion was then added to the 0.6% (w/v) CNF/water suspension (20 mL) under vigorous agitation (800 rpm). After 30 min, the mixture was homogenized in an ultrasonic bath for 30 min. The stirring and sonic treatments were repeated for three times. The composite membrane was obtained by filtration of the mixed suspension on MCE filter, dried at room temperature for 24 h and denoted as CM-1. For comparison, pure CNF membrane, UiO-66/CNF-COOH composite membrane and UiO-66-$NH_2$/CNF-COONa composite membrane were fabricated by the same method with different starting materials and denoted as CM-0, CM-2 and CM-3, respectively.

### 2.4. Characterization

X-ray diffraction (XRD) experiments were carried out by using Rigaku Ultima IV. Fourier transform infrared spectra (FT-IR, Thermo Electron Nicolet-360, USA) were recorded to explore the chemical groups of as-prepared membraned. Scanning electron microscopy (SEM) images were obtained by utilizing a JSM-7600F (JEOL Ltd., Japan). The dimensions of cellulose nanofibrils were detected by

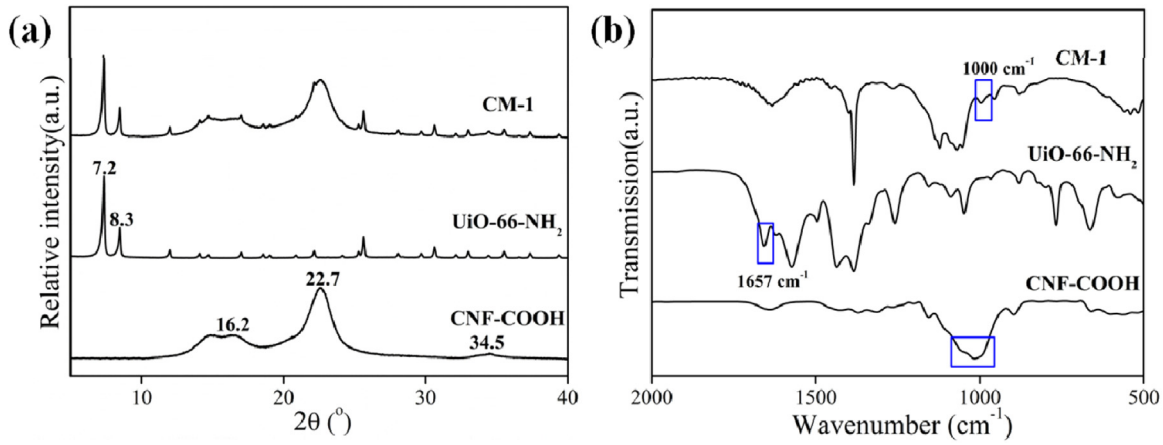


**Fig. 2.** XRD patterns of CNF-COOH, UiO-66-$NH_2$ and CM-1 membrane (a), FT-IR spectra of CNF-COOH, UiO-66, and CM-1 membrane (b).

transmission electron microscopy (TEM, JEM-1400, JEOL, Tokyo, Japan). Atomic force microscopy (AFM, Dimension Edge, Bruker, Germany) was performed to investigate the surface morphology of the membranes. The thickness of the as-prepared membranes was obtained from a micrometer and the final value was calculated from five measurements. Zeta Potential Analyzer (Zetasizer Nano ZS, Malvern Instruments Ltd, UK) was used to reveal the charge of the suspension.

### 2.5. Gas separation experiments

The gas separation performance was measured from the permeances of single gases with a standard apparatus (Fig. S1) at 25 °C [4,13]. Vacuum pump was applied to remove the residual gas in the system. The flux was evaluated with a bubble flow meter. The permeability, Pi (Barrer) is calculated as **Eq.** (1).

$$P_i = N_i l/(A \bullet \Delta pi) \quad (1)$$

where Ni ($cm^3\ s^{-1}$), $l$ (cm), A ($cm^2$) and $\Delta p_i$ (cmHg) refer to the gas flow rate, the film thickness, the membrane area, and the pressure drop, respectively. The ideal selectivity ($S_{ij}$) is acquired from **Eq.** (2).

$$S_{ij} = Pi/Pj \quad (2)$$

## 3. Results and discussions

### 3.1. Membrane characterization

Generally, the TEMPO-mediated process can selectively transform glucosyl units (C6 position) into sodium glucuronosyl groups and break the cellulose chains [22]. As depicted in Fig. 1**a**, the obtained ribbon-like TEMPO-oxidized cotton CNFs possess mostly uniform widths of 4–6 nm and lengths of about 1000 nm. The high aspect ratio of CNFs favors the formation of entangled network in the membranes. CNF-COOH suspension is obtained through the CNF-COONa dispersion via the dilute HCl treatment and the CNFs can be dispersed uniformly through mutual electrostatic repulsion [23]. The suspension presents ultra-high light transparency (inset in Fig. 1**a**) due to the small interstices between the fibrils restrict light scattering [24,25]. Fig. 1**b** displays the SEM morphology of as-synthesized UiO-66-$NH_2$ particles, showing cubic-like structure with an average particle size of ca. 150 nm. The 3D structure of UiO-66-$NH_2$ (inset in Fig. 1**b**) has centric octahedral cages, which is linked with eight corner tetrahedral cages [6,26]. The aperture size of UiO-66-$NH_2$ is suitable for $CO_2$ pass [26]. The quality of starting UiO-66-$NH_2$ particles is further confirmed by $N_2$ sorption (Fig. S2). The UiO-66-$NH_2$ crystals follow type I isotherm with a BET surface area of 737 $m^2/g$.

The CM-1 (CNF-COOH/UiO-66-$NH_2$) composite membrane is fabricated via facile vacuum filtration on a MCE filter with micrometer-sized pores (0.22 μm). The appearance and the morphology of obtained membrane are shown in Fig. 1**c**. The optical observation of the yellow membrane reveals smooth and glossy appearance without noticeable cracks and wrinkles. Generally, the CNFs have a low strain-at-failure under tension, but the obtained membrane is quite damage-tolerant. As displayed in Fig. 1**d**, CM-1 membrane can keep intact without significant cracks when it was bended 180° for several times under the folding tests. The high aspect ratios and entangled network of CNFs impart the membrane excellent mechanical flexibility [27]. TG experiments were conducted to verify the MOF/CNF ratios in the composite membrane (Fig. S3). Results demonstrate that the measured ratio of 1:4.1 is close to the theoretically calculated value of 1:5.

In this study, a designed method was employed to utilize electrostatic interactions as the main driving forces to induce the membrane self-assembly process. The surface charge measurements reflect that the CNF-COOH and UiO-66-$NH_2$ dispersion have zeta potential values of −67 and 41 mV, respectively. Suitable electrostatic repulsion gave rise to the homogeneous dispersion of CNF-COOH [3]. The negatively charged CNF-COOH groups are likely to behave as anchor sites for the positively charged UiO-66-$NH_2$ nanoparticles. The electrostatic force facilitates the incorporation of UiO-66-$NH_2$ into the membrane matrix and restrains the mobilization of MOF particles [2]. The porous MOFs are expected to enhance the permeability of hybrid membranes due to the additional molecular transport pathways created.

The crystalline structure and chemical structure of the CNF/MOF composite membrane were investigated by XRD and FT-IR, respectively. As illustrated in Fig. 2**a**, CNF-COOH preserves typical cellulose I crystalline structure. The TEMPO oxide treatment exerts no influence on the crystalline pattern of cellulose [19]. The diffraction peaks at 16.2°, 22.7° and 34.5° correspond to (110), (200) and (004) planes of cellulose I structure, respectively [28,29]. The XRD pattern for the as-synthesized UiO-66-$NH_2$ shows two sharp peaks at 7.2° and 8.3°, which are in good agreement with the simulated reference for UiO-66-$NH_2$ [2]. In the CM-1 composite membrane, CNF-COOH and UiO-66-$NH_2$ maintain their pristine topology [30]. The strong arc diffractions centered at 22.7° is assigned to the (200) plane of CNFs, proving that the cellulose I crystallites is highly oriented parallel to the membrane surface [20]. The arrangement of CNFs might promote the formation of close-packed layers in the final membranes.

FT-IR experiments were carried out to further explore the composite membranes. According to Fig. 2**b**, the peak from 1503 to 1600 $cm^{-1}$ in the FT-IR spectrum of UiO-66-$NH_2$ is ascribed to stretching vibration of C=O group [31,32]. Comparing FT-IR spectra for UiO-66-$NH_2$ and pristine UiO-66, it is concluded that the main absorption bands assigned to the amine (-$NH_2$) groups are at 1657 $cm^{-1}$ [2]. The striking peak at 1657 $cm^{-1}$ associated with -$NH_2$ group of UiO-66-$NH_2$ is preserved in

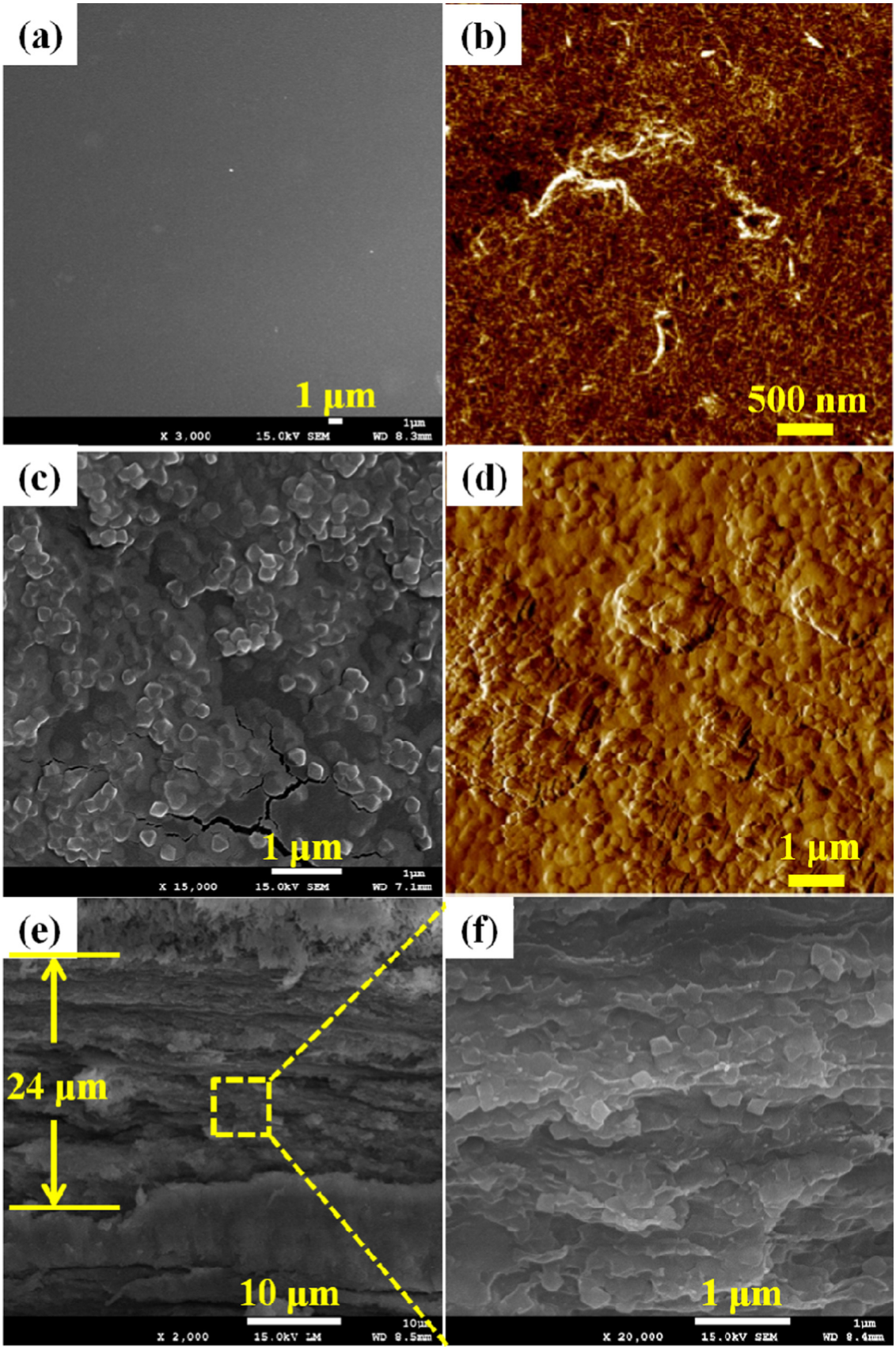


**Fig. 3.** SEM surface and AFM surface images of CM-0 (a and b), CM-1 (c and d); SEM images of cross-section of CM-1 (e and f).

CM-1 membrane. The peak located around 1000 $cm^{-1}$ implies the hydrogen bond interaction between -$NH_2$ group of UiO-66 and -OH group or -COOH group of CNF-COOH, indicating the occurrence of linking reaction and MOFs are chemically linked to the cellulose matrix [33]. The hydrogen bond network can effectively avoid the non-selective space between MOF particles and CNF nanosheets. Moreover, the interaction between -$NH_2$ and -COOH groups confines the MOF particles into restricted area and improve the membrane stability.

SEM cross-section image of the neat CNF membrane (CM-0) is presented in Fig. 3**a**. The surface morphology of CM-0 clearly displays a flat surface without obvious agglomeration. The fracture surface (Fig. S4) of CM-0 is constituted by laminated and densely packed nanolayers. The hydrogen bonds between crystalline CNFs contribute to forming closely packed structure [20]. To obtain more information of pristine CM-0 membrane, AFM image was recorded (Fig. 3**b**). The CNFs are interconnected, tightly cross-linked with each other and paralleled to the membrane surface, which is in agreement with XRD results. CM-0 has a low surface roughness with maximum roughness depth of 6 nm and root mean square roughness of 2 nm. The entangled web-like network makes CNFs a promising polymer matrix for inorganic materials [28].

UiO-66-$NH_2$ nanoparticles can be clearly observed over the CM-1 composite membrane (Fig. 3**c**). The MOF crystals are individually embedded into the membrane and attached tightly with the cellulose matrix. The appeared cracks are generated from the energy of electrons during the SEM imaging process. The optimum arrangement and orientation of CNFs reduce the excessive agglomeration of MOF particles and facilitate attachment and incorporation of UiO-66-$NH_2$. The AFM image of CM-1 (Fig. 3**d**) is highly consistent with SEM observations, confirming that the MOF crystals are uniformly wrapped into the matrix. The homogeneous dispersion of MOFs is further proved by the membrane cross-section. Fig. 3**e and f** roughly visualize laminated CNF nanosheets buried a large number of MOF crystals [34]. As a striking feature, the embedded UiO-66-$NH_2$ nanoparticles in the membrane are entangled with CNFs. No obvious interfacial void is observed as the MOF particles are encapsulated by cellulose layers. Besides, CM-1 exhibits a thickness of ca. 24 μm, and the thickness can be controlled through the rational design of preparation conditions. The introduction of -$NH_2$ groups leads to an improvement in the uniformity of the particle distribution and CNF-MOF adhesion, thus constructing a nearly defect-free interface. The -COOH groups of CNFs react with amino groups in the cellulose matrix to enhance the compatibility between the phase boundaries. The compact and uniform dispersion of UiO-66-$NH_2$ nanoparticles on the membrane matrix offers continuous pathways for $CO_2$ [35,36].

### 3.2. Gas separation tests

The gas-separation performance of the MOF/CNF hybrid membranes are evaluated from the gas permeances of $CO_2$ and $N_2$. The experiments were conducted at steady state and each permeance is kept nearly constant during the measurements. To effectively avoid the swelling and distortion of the crystallographic aperture sizes, a relative small pressure (0.2 MPa) is employed in this study. There is no separation selectivity for $CO_2$ and $N_2$ for bare MCE substrate (pore size, 0.22 μm). As summarized in Table 1, the pristine CM-0 has a $CO_2$ permeability of 7 Barrer with a $CO_2/N_2$ ideal selectivity of 6. Prior studies revealed that self-standing TEMPO-oxidized wood CNF-COONa membranes have free volumes homogeneously present from the membrane surface to inside with an average diameter of 0.47 nm [22]. In contrast, the average hole diameters present between nanofibrils in the cotton CNF-COOH layers may be somewhat smaller due to the prevailing inter-and intra fibril hydrogen bond network. The small pore size of the membrane and the crystalline structures of CNFs are probably responsible for the high $N_2$-barrier properties. The $N_2$ molecules are likely to pass through the CNF layers via the traditional diffusion mechanism. The $CO_2$ permeability is relatively higher than $N_2$, suggesting that the solubility factor of $CO_2$ molecules may not be negligible. The introduction of MOF particles (UiO-66 or UiO-66-$NH_2$) results enhanced gas permeability of $N_2$ and $CO_2$ with a simultaneous increase in selectivity. CM-1 (UiO-66-$NH_2$/CNF-COOH) has a $CO_2$ permeability of 139 Barrer and a $CO_2/N_2$ ideal selectivity of 46. These values are comparable to those previously reported for UiO-66-$NH_2$/polymer composite membranes (Fig. S5) and other cellulose derived gas-separation materials (Table S1) [26,37,38]. In addition, the preparation procedures have good reproducibility and the membranes prepared using the same protocol present similar permeability and selectivity values (an allowable error of ± 3%).

**Table 1**
Comparison of single gas permeance over different membranes.

| Sample | Permeability (Barrer) | | Ideal selectivity ($CO_2/N_2$) |
|---|---|---|---|
| | $CO_2$ | $N_2$ | |
| CM-0 | 7 ± 0.6 | 1.2 ± 0.1 | 6 ± 0.4 |
| CM-1 | 139 ± 1.2 | 3.1 ± 0.1 | 46 ± 2.6 |
| CM-2 | 50 ± 0.9 | 1.8 ± 0.1 | 28 ± 1.2 |
| CM-3 | 29 ± 0.4 | 2.6 ± 0.2 | 11 ± 0.7 |

Three factors contribute strongly to the superior performance of CM-1: (a) close interfacial contact derived from acid-base interaction (-$NH_2$ and –COOH groups) avoids the formation of non-selective gaps; (b) CNF-COOH cross-links the amine groups leading to well-dispersion of UiO-66-$NH_2$ among CNF layers and (c) the high permeance and affinity of nanoporous UiO-66-$NH_2$ for $CO_2$ due to the interaction between $CO_2$ and -$NH_2$ groups [39]. Amino groups can act as non-ionic $CO_2$ carriers through covalently connected to cellulose chains and facilitate $CO_2$ transport. To clarify that and provide more evidence, CM-2 (UiO-66/CNF-COOH) and CM-3 (UiO-66-$NH_2$/CNF-COONa) composite membrane were prepared as controlling samples. CM-2 shows a $CO_2$ permeability of 50 Barrer and a $CO_2/N_2$ ideal selectivity of 28. The CNF nanolayers are densely packed and the intercalation of UiO-66 particles enlarges the CNF layers to offer fast pathways for gas molecules. And CM-2 exerts a better separation performance than that of neat CNF membrane. However, the lack of amine groups and poor interfacial adhesion limits its further boost in performance. CM-3 composite membrane has a $CO_2$ permeability of 29 Barrer with a $CO_2/N_2$ ideal selectivity of 11. The relatively high $CO_2$ permeance is assigned to the functional -$NH_2$ groups, which provide more $CO_2$ adsorption sites and increase the affinity toward $CO_2$ [40,41]. Trade-off effect between gas flux and separation performance has been reported as each upper bound in the famous 2008 Robeson curve [42,43]. The designer CM-1 membrane breaks the trade-off relationship between permeability and selectivity due to high affinity and nearly ideal compatibility between MOFs and CNFs.

The combination of UiO-66-$NH_2$ and CNF-COOH prevents gas leakage at the interface and gives high flux and selectivity of $CO_2$. As illustrated in Fig. 4, a possible mechanism is proposed. The intercalation of UiO-66-$NH_2$ expands the CNF layers, providing fast pathways for gas molecules. Porous $CO_2$-philic UiO-66-$NH_2$ prefers the passage of $CO_2$ molecules with a lower hindrance [6,26]. Amino groups are the typical non-ionic $CO_2$ carriers. Moreover, the favorable acid-base interaction between UiO-66-$NH_2$ and CNF-COOH nanosheets promotes close interfacial contact. The high affinity and good compatibility result connective pathways for $CO_2$ [9,44,45].

## 4. Conclusion

In this study, MOF/CNF composite membranes were constructed via a facile vacuum filtration over MCE support. The membrane is prepared by using UiO-66-$NH_2$ as dispersed nanoparticles and CNF-COOH as the continuous phase and cross-linking agents. The contribution of the

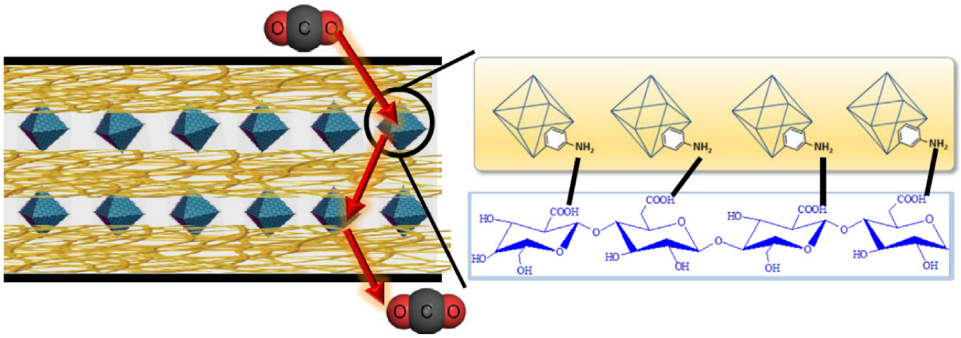


**Fig. 4.** Mechanism illustration of the transport of $CO_2$.

inter-molecular MOF/CNF interaction is discussed. CNF-COOH cross-links UiO-66-$NH_2$ nanoparticles, leading to homogeneous dispersion of MOFs and excellent compatibility with cellulose matrix. The acid-base interaction and electrostatic force formed between UiO-66-$NH_2$ and CNF-COOH nanosheets promotes the close interfacial contact and ideal interfacial morphology. The optimum separation performance was achieved over CM-1 (UiO-66-$NH_2$/CNF-COOH) with a $CO_2$ permeability of 139 Barrer and a $CO_2/N_2$ selectivity ratio of 46. The functional -$NH_2$ groups of CM-1 membranes is considered as crucial factor governing the $CO_2$ transport behavior. The strategy of incorporating MOFs into cellulose matrix through chemical bonding is promising in fabricating high performance separation membranes.

## Acknowledgments

The authors are grateful for the financial support of China Postdoctoral Science Foundation (2017M611824), Natural Science Key Project of the Jiangsu Higher Education Institutions (15KJA220001) and Priority Academic Program Development of Jiangsu Higher Education Institutions (PAPD).

## Appendix A. Supporting information

Supplementary data associated with this article can be found in the online version at doi:10.1016/j.memsci.2018.09.055.

## References

[1] J. Yao, H. Wang, Zeolitic imidazolate framework composite membranes and thin films: synthesis and applications, Chem. Soc. Rev. 43 (2014) 4470–4493.
[2] M. Jia, Y. Feng, S. Liu, J. Qiu, J. Yao, Graphene oxide gas separation membranes intercalated by UiO-66-$NH_2$ with enhanced hydrogen separation performance, J. Membr. Sci. 539 (2017) 172–177.
[3] J. Yao, K. Wang, M. Ren, J.Z. Liu, H. Wang, Phase inversion spinning of ultrafine hollow fiber membranes through a single orifice spinneret, J. Membr. Sci. 421 (2012) 8–14.
[4] L. Sheng, C. Wang, F. Yang, L. Xiang, X. Huang, J. Yu, L. Zhang, Y. Pan, Y. Li, Enhanced $C_3H_6/C_3H_8$ separation performance on MOF membranes through blocking defects and hindering framework flexibility by silicone rubber coating, Chem. Commun. 53 (2017) 7760–7763.
[5] F. Luo, C. Yan, L. Dang, R. Krishna, W. Zhou, H. Wu, X. Dong, Y. Han, T.L. Hu, M. O'Keeffe, L. Wang, M. Luo, R.B. Lin, B. Chen, UTSA-74: a MOF-74 isomer with two accessible binding sites per metal center for highly selective gas separation, J. Am. Chem. Soc. 138 (2016) 5678–5684.
[6] S. Castarlenas, C. Tellez, J. Coronas, Gas separation with mixed matrix membranes obtained from MOF UiO-66-graphite oxide hybrids, J. Membr. Sci. 526 (2017) 205–211.
[7] J. Park, M. Oh, Construction of flexible metal-organic framework (MOF) papers through MOF growth on filter paper and their selective dye capture, Nanoscale 9 (2017) 12850–12854.
[8] A. Donnadio, R. Narducci, M. Casciola, F. Marmottini, R. D'Amato, M. Jazestani, H. Chiniforoshan, F. Costantino, Mixed membrane matrices based on Nafion/UiO-66/$SO_3$H-UiO-66 Nano-MOFs: revealing the effect of crystal size, sulfonation, and filler loading on the mechanical and conductivity properties, ACS Appl. Mater. Interfaces 9 (2017) 42239–42246.
[9] X. Cheng, Z. Jiang, X. Cheng, H. Yang, L. Tang, G. Liu, M. Wang, H. Wu, F. Pan, X. Cao, Water-selective permeation in hybrid membrane incorporating multi-functional hollow ZIF-8 nanospheres, J. Membr. Sci. 555 (2018) 146–156.
[10] M. Matsumoto, T. Kitaoka, Ultraselective gas separation by nanoporous Metal-organic frameworks embedded in gas-barrier nanocellulose films, Adv. Mater. 28 (2016) 1765–1769.
[11] S. Friebe, B. Geppert, F. Steinbach, J. Caro, Metal-organic framework UiO-66 Layer: a highly oriented membrane with good selectivity and hydrogen permeance, ACS Appl. Mater. Interfaces 9 (2017) 12878–12885.
[12] E. Barankova, X. Tan, L.F. Villalobos, E. Litwiller, K.V. Peinemann, A metal chelating porous polymeric support: the missing link for a defect-free metal-organic framework composite membrane, Angew. Chem. Int. Ed. 56 (2017) 2965–2968.
[13] S. Biswas, J. Zhang, Z. Li, Y.-Y. Liu, M. Grzywa, L. Sun, D. Volkmer, P. Van der Voort, Enhanced selectivity of $CO_2$ over $CH_4$ in sulphonate-, carboxylate- and iodo-functionalized UiO-66 frameworks, Dalton Trans. 42 (2013) 4730–4737.
[14] M.A. Rodrigues, Jd.S. Ribeiro, Ed.S. Costa, J.L. de Miranda, H.C. Ferraz, Nanostructured membranes containing UiO-66 (Zr) and MIL-101 (Cr) for $O_2/N_2$ and $CO_2/N_2$ separation, Sep. Purif. Technol. 192 (2018) 491–500.
[15] Y. Habibi, Key advances in the chemical modification of nanocelluloses, Chem. Soc. Rev. 43 (2014) 1519–1542.
[16] R.J. Moon, A. Martini, J. Nairn, J. Simonsen, J. Youngblood, Cellulose nanomaterials review: structure, properties and nanocomposites, Chem. Soc. Rev. 40 (2011) 3941–3994.
[17] X.F. Zhang, T. Hou, J. Chen, Y. Feng, B.G. Li, X.L. Gu, M. He, J.F. Yao, Facilitated transport of $CO_2$ through the transparent and flexible cellulose membrane promoted by fixed-site carrier, ACS Appl. Mater. Interfaces 10 (2018) 24930–24936.
[18] X.-F. Zhang, Y. Feng, C. Huang, Y. Pan, J. Yao, Temperature-induced formation of cellulose nanofiber film with remarkably high gas separation performance, Cellulose 24 (2017) 5649–5656.
[19] M. Shimizu, T. Saito, A. Isogai, Water-resistant and high oxygen-barrier nanocellulose films with interfibrillar cross-linkages formed through multivalent metal ions, J. Membr. Sci. 500 (2016) 1–7.
[20] Q.L. Yang, T. Saito, L.A. Berglund, A. Isogai, Cellulose nanofibrils improve the properties of all-cellulose composites by the nano-reinforcement mechanism and nanofibril-induced crystallization, Nanoscale 7 (2015) 17957–17963.
[21] Y. He, H. Jin, S. Qiu, Q. Li, A novel strategy for high-performance transparent conductive films based on double-walled carbon nanotubes, Chem. Commun. 20 (2017) 53–59.
[22] S. Fujisawa, Y. Okita, H. Fukuzumi, T. Saito, A. Isogai, Preparation and characterization of TEMPO-oxidized cellulose nanofibril films with free carboxyl groups, Carbohydr. Polym. 84 (2011) 579–583.
[23] W. Yang, H. Bian, L. Jiao, W. Wu, Y. Deng, H. Dai, High wet-strength, thermally stable and transparent TEMPO-oxidized cellulose nanofibril film via cross-linking with poly-amide epichlorohydrin resin, RSC Adv. 7 (2017) 31567–31573.
[24] J. Huang, H. Zhu, Y. Chen, C. Preston, K. Rohrbach, J. Cumings, L. Hu, Highly transparent and flexible nanopaper transistors, ACS Nano 7 (2013) 2106–2113.
[25] H. Zhu, Z. Fang, C. Preston, Y. Li, L. Hu, Transparent paper: fabrications, properties, and device applications, Energy Environ. Sci. 7 (2014) 269–287.
[26] T.-B. Nguyen, D. Rodrigue, S. Kaliaguine, In-situ cross interface linking of PIM-1 polymer and UiO-66-$NH_2$ for outstanding gas separation and physical aging control, J. Membr. Sci. 548 (2018) 429–438.
[27] C.-N. Wu, T. Saito, S. Fujisawa, H. Fukuzumi, A. Isogai, Ultrastrong and high gas-barrier nanocellulose/clay-layered composites, Biomacromolecules 13 (2012) 1927–1932.
[28] H. Fukuzumi, T. Saito, T. Wata, Y. Kumamoto, A. Isogai, Transparent and high gas barrier films of cellulose nanofibers prepared by TEMPO-mediated oxidation, Biomacromolecules 10 (2009) 162–165.
[29] H. Fukuzumi, T. Saito, A. Isogai, Influence of TEMPO-oxidized cellulose nanofibril length on film properties, Carbohydr. Polym. 93 (2013) 172–177.
[30] Q. Yang, H. Fukuzumi, T. Saito, A. Isogai, L. Zhang, Transparent cellulose films with high gas barrier properties fabricated from aqueous alkali/urea solutions, Biomacromolecules 12 (2011) 2766–2771.
[31] G.W. Peterson, A.X. Lu, T.H. Epps III, Tuning the morphology and activity of electrospun polystyrene/UiO-66-$NH_2$ Metal-organic framework composites to enhance chemical warfare agent removal, ACS Appl. Mater. Interfaces 9 (2017) 32248–32254.
[32] H. Fukuzumi, T. Saito, S. Iwamoto, Y. Kumamoto, T. Ohdaira, R. Suzuki, A. Isogai, Pore size determination of TEMPO-oxidized cellulose nanofibril films by positron annihilation lifetime spectroscopy, Biomacromolecules 12 (2011) 4057–4062.

[33] R. Ning, C.-N. Wu, M. Takeuchi, T. Saito, A. Isogai, Preparation and characterization of zinc oxide/TEMPO-oxidized cellulose nanofibril composite films, Cellulose 24 (2017) 4861–4870.
[34] T. Kurihara, A. Isogai, The effect of electric charge density of polyacrylamide (PAM) on properties of PAM/cellulose nanofibril composite films, Cellulose 22 (2015) 499–506.
[35] X. Zhao, Y. Su, Y. Liu, Y. Li, Z. Jiang, Free-standing graphene oxide-palygorskite nanohybrid membrane for oil/water separation, ACS Appl. Mater. Interfaces 8 (2016) 8247–8256.
[36] C. Jiang, T.Y. Cao, W.J. Wu, J.L. Song, Y.C. Jin, Novel approach to prepare ultrathin lignocellulosic film for monitoring enzymatic hydrolysis process by quartz crystal microbalance, ACS Sustain Chem. Eng. 5 (2017) 3837–3844.
[37] X. Wu, W. Liu, H. Wu, X. Zong, L. Yang, Y. Wu, Y. Ren, C. Shi, S. Wang, Z. Jiang, Nanoporous ZIF-67 embedded polymers of intrinsic microporosity membranes with enhanced gas separation performance, J. Membr. Sci. 548 (2018) 309–318.
[38] M. Vinoba, M. Bhagiyalakshmi, Y. Alqaheem, A.A. Alomair, A. Pérez, M.S. Rana, Recent progress of fillers in mixed matrix membranes for $CO_2$ separation: a review, Sep. Purif. Technol. 188 (2017) 431–450.
[39] P.Q. Liao, D.D. Zhou, A.X. Zhu, L. Jiang, R.B. Lin, J.P. Zhang, X.M. Chen, Strong and dynamic $CO_2$ sorption in a flexible porous framework possessing guest chelating claws, J. Am. Chem. Soc. 134 (2012) 17380–17383.
[40] Y.H. Jung, T.H. Chang, H.L. Zhang, C.H. Yao, Q.F. Zheng, V.W. Yang, H.Y. Mi, M. Kim, S.J. Cho, D.W. Park, H. Jiang, J. Lee, Y.J. Qiu, W.D. Zhou, Z.Y. Cai, S.Q. Gong, Z.Q. Ma, High-performance green flexible electronics based on biodegradable cellulose nanofibril paper, Nat. Commun. 6 (2015) 7170–7175.
[41] L. Zhang, L. Xiang, C. Hang, W. Liu, W. Huang, Y. Pan, From discrete molecular cages to a network of cages exhibiting enhanced $CO_2$ adsorption capacity, Angew. Chem. Int. Ed. 56 (2017) 7787–7791.
[42] S. Wang, Y. Liu, M. Zhang, D. Shi, Y. Li, D. Peng, G. He, H. Wu, J. Chen, Z. Jiang, Comparison of facilitated transport behavior and separation properties of membranes with imidazole groups and zinc ions as $CO_2$ carriers, J. Membr. Sci. 505 (2016) 44–52.
[43] X. Xu, J. Zhou, L. Jiang, G. Lubineau, T. Ng, B.S. Ooi, H.-Y. Liao, C. Shen, L. Chen, J.Y. Zhu, Highly transparent, low-haze, hybrid cellulose nanopaper as electrodes for flexible electronics, Nanoscale 8 (2016) 12294–12306.
[44] G. Liu, Z. Jiang, K. Cao, S. Nair, X. Cheng, J. Zhao, H. Gomaa, H. Wu, F. Pan, Pervaporation performance comparison of hybrid membranes filled with two-dimensional ZIF-L nanosheets and zero-dimensional ZIF-8 nanoparticles, J. Membr. Sci. 523 (2017) 185–196.
[45] T. Puspasari, N. Pradeep, K.V. Peinemann, Crosslinked cellulose thin film composite nanofiltration membranes with zero salt rejection, J. Membr. Sci. 491 (2015) 132–137.